Scaling towards the critical point in the combined reaction/Gibbs ensemble

Polat, H.M.; Lasala, Silvia; De Meyer, Frédérick; Houriez, Céline; Moultos, O.; Vlugt, T.J.H.

Citation (APA)
Polat, H. M., Lasala, S., De Meyer, F., Houriez, C., Moultos, O., & Vlugt, T. J. H. (2024). Scaling towards the critical point in the combined reaction/Gibbs ensemble. *Fluid Phase Equilibria*, *582*, Article 114084. https://doi.org/10.1016/j.fluid.2024.114084
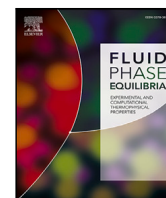
Important note
To cite this publication, please use the final published version (if applicable).
Please check the document version above.

Scaling towards the critical point in the combined reaction/Gibbs ensemble

H. Mert Polat [a], Silvia Lasala [b], Frédéric de Meyer [c,d], Céline Houriez [d], Othonas A. Moultos [a], Thijs J.H. Vlugt [a,*]

[a] Engineering Thermodynamics, Process & Energy Department, Faculty of Mechanical Engineering, Delft University of Technology, Leeghwaterstraat 39, Delft 2628CB, The Netherlands
[b] Université de Lorraine, Laboratoire Réactions et Génie des Procédés, 54000 Nancy, France
[c] CO$_2$ and Sustainability R&D Program, Gas & Low Carbon Entity, OneTech, TotalEnergies S.E., 92078 Paris, France
[d] Mines Paris, PSL University, Center for Thermodynamics of Processes (CTP), 77300 Fontainebleau, France

ARTICLE INFO

ABSTRACT

We explore the impact of force field parameters and reaction equilibrium on the scaling behavior towards the critical point in reactive binary systems, focusing on NO_2/N_2O_4. This system can be considered as a special single-component system since NO_2 and N_2O_4 are in chemical equilibrium via the chemical reaction $2NO_2 \rightleftharpoons N_2O_4$. We simplify the system by representing both components as single LJ particles, achieving excellent agreement with densities computed using molecular simulations in which all-atom force fields were used. We investigate the effect of force field parameters (ϵ and σ) on phase behavior and show that the critical exponent β remains constant, which means that intermolecular interactions do not affect the scaling to the critical point when the chemical reaction takes place. We also investigate the sensitivity of the reaction equilibrium constant and show that even small changes in isolated molecule partition functions lead to large differences in chemical equilibria. We show that the critical exponent β is different for systems with different reaction equilibrium constants, so a careful parameterization of β is needed for an accurate computation of critical temperatures of reactive mixtures. We perform a screening of reactive binary mixtures for a wide range of ideal gas reaction equilibrium constants, revealing key insights into the thermodynamic behavior and critical properties. Thereby we facilitate the efficient screening of reactive binary mixtures for various applications. Our results emphasize the importance of accurately parameterizing β and provide valuable insights into the critical scaling behavior of complex reactive systems.

1. Introduction

Reactive mixtures, characterized by the occurance of chemical reactions between their components, have caught the attention of researchers across diverse scientific and engineering disciplines [1–8]. These mixtures are very interesting due to the intricate interplay between chemical reactions and physical interactions, leading to unique phase behaviors and thermodynamic properties [5,9]. Reactive working fluids have the potential to improve the thermodynamic efficiency of thermodynamic cycles, such as Brayton cycles, beyond that of conventional nonreactive fluids [10–14]. Reactive working fluids have been shown to increase power plant efficiencies [13] and the performance of heat pumps [14]. An important example of such a system is the binary mixture composed of nitrogen dioxide (NO_2) and dinitrogen tetroxide (N_2O_4). Reactive mixtures find applications in a wide range of domains, e.g., in aerospace industry, where NO_2/N_2O_4 mixtures serve as vital components in rocket propulsion [15–17], in environmental

science, where their presence in atmospheric chemistry impacts air quality [2,4,18], and in climate change studies [5,6,19]. In the two-phase region, this binary mixture has similar phase characteristics as a single-component system (i.e., a unique critical point and a unique saturation pressure-temperature curve), due to the presence of a fast chemical reaction [5,9,20,21]:

$$2NO_2 \rightleftharpoons N_2O_4 \tag{R1}$$

In this system, the decomposition of NO_2 into NO and O_2 also occurs. However, this reaction is not considered in our study as it is only relevant at high temperatures [22].

Previous Monte Carlo simulation studies have made significant contributions to the understanding of reactive systems. Johnson et al. [23] introduced Monte Carlo (MC) simulations combining Reaction Ensemble (RE) and Gibbs Ensemble (GE), and investigated the dimerization

of NO_2, showing an excellent agreement with experimental compositions and densities for both the liquid and gas phase. Recently, Lasala et al. [21] performed all-atom MC simulations in the combined RE/GE ensemble and used the Peng-Robinson equation of state with advanced mixing rules [24] to study the NO_2/N_2O_4 system. These authors achieved excellent agreement between RE/GEMC simulations and experiments, especially in determining critical temperatures and critical densities [21].

Understanding the scaling of liquid and gas phase densities towards the critical point in reactive mixtures, such as NO_2/N_2O_4, is of significant interest because it provides crucial insights into the intricate interplay between intermolecular interactions and chemical equilibria, offering valuable information for optimizing thermodynamic cycles and processes in various applications. The Vapor-Liquid Equilibrium (VLE) curve of the NO_2/N_2O_4 system is well-established in literature [8,9,25–27]. However, the scaling of the gas- and liquid phase densities as the system approaches the critical point is not well characterized. RE/GEMC simulations are an ideal method to study the scaling towards the critical point as the phase equilibrium and the chemical equilibrium are simultaneously obtained [23,28,29]. The VLE curve of reactive mixtures is determined by the interplay between (1) the intermolecular interactions dictated by the force field, and (2) the isolated molecule partition functions of reactants and reaction products that define the reaction equilibrium in the ideal gas phase. While RE/GEMC simulations offer a method for studying the interplay between intermolecular interactions and reaction equilibria, there are alternative approaches to investigate VLEs using molecular simulations. For example, multiple histogram reweighting in combination with grand-canonical MC provides higher accuracies, especially close to the critical point [30–36]. However, the RE/GEMC simulations, known for their simplicity and ease of implementation, offer practical means to investigate VLEs when fast chemical reactions also take place [37]. Using RE/GEMC simulations, we can investigate how the interactions between the molecules or the reaction equilibria influence the scaling towards the critical point. The scaling can be investigated by fitting the temperature dependence of the difference in densities of liquid and gas phases to a scaling law [36,38]:

$$\left(\frac{\rho_l - \rho_g}{\rho_0} \right)^{\frac{1}{\beta}} = B(T - T_c) \tag{1}$$

where ρ_l and ρ_g are the number densities of liquid and gas phases, respectively, ρ_0 is an arbitrary number density to make the left hand side of Eq. (1) dimensionless (it has the same units as ρ_l and ρ_g, here set to $1 \, \text{Å}^{-3}$), B is a system dependent fitting parameter, T is absolute temperature, T_c is critical temperature, and β is the critical exponent. The value of β varies between 0.31–0.33 (depending slightly on the shape of the molecules), which was established for single-component systems [36,39–42]. It remains an open question whether the values between 0.31–0.33 for the critical exponent β hold for binary mixtures that effectively behave as a single component system due to the presence of chemical reactions. To estimate the density at the critical point, the average mass density of the liquid and gas phases can be fitted to the law of rectilinear diameters [36,43]:

$$\frac{\rho_l + \rho_g}{2} = \rho_c + A(T - T_c) \tag{2}$$

where ρ_c is the critical density and A is a system dependent fitting parameter. Note that in principle, both number and mass densities of liquid and gas phases can be used to investigate the scaling towards the critical point using Eq. (2). For single-component systems, this is not important as the mass density is simply the product of number density and molar mass of that component. In a binary mixture with a dimerization reaction such as reaction R1, the number density of the dimer must be counted twice when computing the mass density of the mixture because the molar mass of the dimer is twice that of the monomer. Here, we investigate both options. Eq. (2) shows that

accurate estimations of critical temperatures are crucial for obtaining accurate critical densities. For phase equilibria of non-reactive binary mixtures, Wichterle et al. [44] proposed the following scaling of the compositions towards the critical point.

$$\left(X_i - Y_i \right)^{\frac{1}{\beta}} = C(T - T_c) \tag{3}$$

where X_i and Y_i are the mole fractions of one of the components in the liquid and gas phases, respectively, C is a system dependent fitting parameter, and β is the same critical exponent as in Eq. (1).

In this study, we investigate how the intermolecular interactions and isolated molecule partition functions affect the scaling of reactive mixtures towards the critical point, and particularly the critical exponent β. By investigating the effect of intermolecular interactions and isolated molecule partition functions, we aim to refine our understanding of the scaling towards the critical point. To simplify and improve the computational efficiency of our simulations, we treat both NO_2 and N_2O_4 molecules as single LJ interaction sites. We investigate the effect of different force field parameters (ϵ and σ) and reaction equilibria (by modifying the values of the isolated molecule partition functions of molecules) on the value of the critical exponent β. As there are different chemical compounds forming dimers in the gas phase such as aluminum chloride [1,45,46] and aluminum bromide [45–47], and each compound that forms dimers in the gas phase may be considered as a potential working fluid in a thermodynamic cycle, systematic knowledge about the scaling towards the critical point in reactive binary systems is needed. Therefore, we conduct a comprehensive screening study to explore the values of β, T_c, and ρ_c for monomer/dimer pairs with different ideal gas reaction equilibrium constants. Our findings not only contribute to our understanding of the critical exponent β, but also provide invaluable insights into the critical scaling behavior of complex reactive systems. The screening we conducted can be used as a predictive tool to calculate the critical point of different reactive binary mixtures. These findings may have significant implications for diverse scientific and engineering disciplines such as energy technology [48] and design of chemical processes [49,50], where accurate modeling of phase behavior is critical.

This article is organized as follows: the simulation methods are explained in Section 2, while we discuss the results from our simulations in Section 3. Our key findings include insensitivity of the values of the critical exponents β to force field parameters, the requirement of a specific value of β for accurate estimations of critical temperatures in the presence of chemical reactions, and how the values of β, T_c, and ρ_c change as a function of the temperature dependence of ideal gas reaction equilibrium constants. The main results of our study are summarized in Section 4.

2. Simulation methods

All simulations are performed using an in-house MC simulation code [51] which combines RE [29] with GE [52–54] to compute phase and chemical equilibria simultaneously, as shown earlier by Johnson et al. [23]. Fig. 1 shows that this ensemble (RE/GE) samples the phase space by allowing particle and volume exchanges between two simulation boxes and the chemical space by attempting chemical reactions in the forward or reverse direction [23]. The equilibrium condition for a chemical reaction is [55]:

$$\sum_{i=1}^{S} \nu_i \mu_i = 0 \tag{4}$$

where S is the number of species involved in the reaction, ν_i is the stoichiometric coefficient of species i in the reaction, and μ_i is the chemical potential of species i. Here, we consider the stoichiometric coefficients of the reactants negative, while the reaction products have positive stoichiometric coefficients ($\nu_i = 0$ if species i does not take
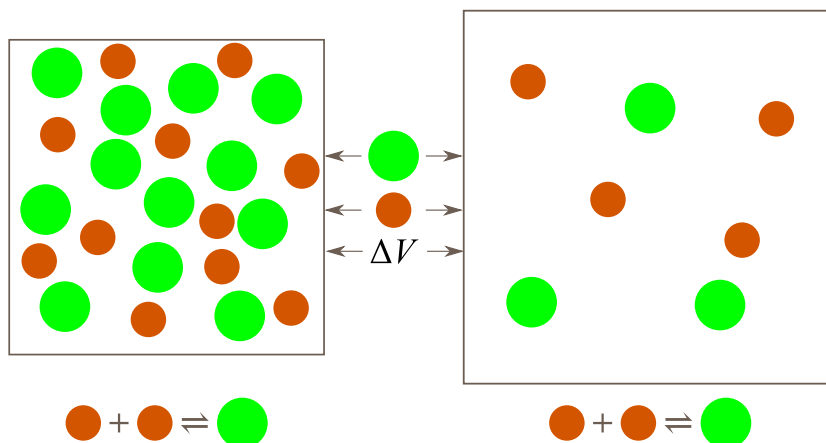
Fig. 1. Schematic representation of our RE/GEMC simulations as introduced by Johnson et al. [23]. The combination of RE and GE (NVT version) allows us to sample phase equilibrium by particle (Eq. (7)) and volume (Eq. (8)) exchanges between two simulation boxes and chemical equilibrium by attempting reaction trial moves in forward or reverse directions (i.e. a trial move in which reactants are removed and reaction products are inserted at random positions in the simulation box, Eq. (9)). This simulation technique ensures that the pressures of the two simulation boxes are equal ($P^1 = P^2$), the chemical potentials of the same species i in the two simulation boxes are equal ($\mu_i^1 = \mu_i^2$), and the equilibrium conditions hold for all reactions in the system (Eq. (4)).

part in the reaction). The chemical potential of species i is defined as [37,56]:

$$\mu_i = \mu_i^0 + k_B T \ln\left[\frac{\rho_i}{\rho_0}\right] + \mu_i^{ex} \qquad (5)$$

where μ_i^0 is the ideal gas standard state chemical potential of species i, k_B is the Boltzmann constant, T is absolute temperature, ρ_i is the number density of species i, and μ_i^{ex} is the excess chemical potential of species i. By adding the first two terms of the right-hand side of Eq. (5) we obtain the ideal gas chemical potential of species i ($\mu_i^{IG} = \mu_i^0 + k_B T \ln\left[\frac{\rho_i}{\rho_0}\right]$) where μ_i^0 is defined as [56]:

$$\mu_i^0 = -k_B T \ln\left[\frac{q_i}{\Lambda_i^3 \rho_0}\right] \qquad (6)$$

where q_i is the isolated molecule partition function of species i (with the translational part excluded) and Λ_i is the thermal De Broglie wavelenght of species i.

For transferring a particle of species i from box 1 to box 2, the acceptance criterion is [28,36]:

$$acc(o \to n) = \min\left[1, \frac{N_{i,1} V_2}{(N_{i,2} + 1) V_1} \exp\left[-\frac{\Delta U}{k_B T}\right]\right] \qquad (7)$$

where $N_{i,j}$ is the number of particles of species i in simulation box j, V_j is the volume of simulation box j, and ΔU is the difference in potential energies of the new (n) and old (o) configurations ($U_n - U_o$). Eq. (7) implies the following way of selecting the particle that is transferred between two simulation boxes [57]: (1) the source and target simulation boxes are selected at random, (2) a target species is selected at random, and (3) a particle of the target species in the target simulation box is selected at random. For a volume exchange at constant total volume of the simulation boxes, the acceptance criterion is [28,36]:

$$acc(o \to n) = \min\left[1, \exp\left[-\frac{\Delta U}{k_B T} + N_1 \frac{V_{n,1}}{V_{o,1}} + N_2 \frac{V_{n,2}}{V_{o,2}}\right]\right] \qquad (8)$$

where N_j is the total number of particles in simulation box j, and $V_{n,j}$ and $V_{o,j}$ are the new and old volumes of the simulation box j, respectively. For a trial move in which reactant molecules in box j are removed and reaction products are inserted at random positions in simulation box j, the acceptance criterion is [23,29,58]:

$$acc(o \to n) = \min\left[1, \prod_{i=1}^{S} \frac{N_{i,j}!}{(N_{i,j} + \nu_i)!} \prod_{i=1}^{S} \left(\frac{V_j q_i}{\Lambda_i^3}\right)^{\nu_i} \exp\left[-\frac{\Delta U}{k_B T}\right]\right] \qquad (9)$$

where V_j is the volume of simulation box j. Eq. (9) implies the following way of selecting the reactants: (1) the target simulation box is selected at random, (2) the direction of the reaction is selected at random (forward or reverse directions have 50% probability each to get selected), and (3) the target reactant particles are selected at random. In principle, reaction trial moves are only required to be performed in the gas phase [21]. In this case, due to phase equilibrium between two simulation boxes (resulting from particle and volume exchanges), chemical equilibrium is also achieved in the liquid phase. Note that the term $\prod_{i=1}^{S} \left(\frac{V_j q_i}{\Lambda_i^3}\right)^{\nu_i}$ in Eq. (9) is closely related to ideal gas reaction equilibrium constant K_{IG} (i.e. the equilibrium constant where intermolecular interactions are absent) as [59,60]:

$$K_{IG} = \prod_{i=1}^{S} q_i^{\nu_i} = \prod_{i=1}^{S} \rho_i^{\nu_i} \qquad (10)$$

where ρ_i is the number density of species i.

In our simulations, single LJ particles are used for simplicity. The intermolecular interactions between two particles are computed using a 12-6 LJ potential. The force field parameters for unlike particles ($\varepsilon_{i,j}$ and $\sigma_{i,j}$) are computed using the Lorentz–Berthelot mixing rule [36]. The interactions are truncated and shifted (no tail corrections) at a distance of $2.5\sigma_{i,j}$ where $\sigma_{i,j}$ is the distance where the potential energy between species i and j is zero. In this way, each pure component has the same VLE phase diagram in reduced units. Initial configurations were generated by randomly inserting molecules in two simulation boxes. An initial system size of 1000 molecules is used unless specified otherwise. For all simulations, 2×10^5 equilibration cycles and 10^6 production cycles were performed. In each MC cycle, the number of MC trial moves was equal to the total number of molecules in the two simulation boxes. In our RE/GE simulations, we used particle displacements (79%), particle exchanges (10%), volume exchanges (1%), and reaction (10%) trial moves with fixed probabilities. In single-component GE simulations, particle displacements (89%), particle exchanges (10%), and volume exchanges (1%) are used with fixed probabilities. We consider 3-dimensional periodic boundary conditions. Maximum particle- and volume changes are set to values so that ca. 50% of trial moves are accepted.

We optimize the critical exponent β (Eq. (1)) by systematically evaluating β in the range of 0.1–0.5 and computing the coefficients of determination (R^2) [61] for the linear regression fits to the terms $\left(\frac{\rho_l - \rho_g}{\rho_0}\right)^{\frac{1}{\beta}}$ as a function of temperature. The critical exponent β is determined by selecting the value of β that corresponds to the maximum

of R^2. We then compute the value of T_c by extrapolating the linear regression fit to the terms $\left(\frac{\rho_l-\rho_g}{\rho_0}\right)^{\frac{1}{\beta}}$ to zero as the difference between ρ_l and ρ_g is zero at critical point by definition. To assess the error in the estimate of β, we estimate T_c for a range of β values, centering around the best fit value of β, and identify the interval in which the estimations of T_c exhibit maximum deviations of 1% from T_c computed using the estimate of β. Earlier work by Martin and Siepmann [42] showed that the LJ interaction parameters (ϵ and σ) for an interaction site cannot be determined beyond an accuracy of 1% using GEMC simulations. Messerly et al. [62] investigated the uncertainties in LJ force field parameters for *n*-alkanes by conducting GEMC simulations for an extensive set of LJ parameters. The recommended values of ϵ and σ for CH_3 and CH_2 groups in an *n*-alkane molecule have uncertainties between 0.2%–3%, while the computed values of T_c have uncertainties in the range of 0.6–1.9% [62]. Although the computed values of ρ_l and ρ_g also have uncertainties, these uncertainties are much lower than 1%. For this reason, a threshold of 1% for T_c was chosen for a given molecular system (since the value of T_c scales with ϵ). For the remainder of this study, the errors in β for different systems are shown as subscripts.

3. Results and discussion

3.1. Mapping the NO_2/N_2O_4 system to LJ particles

In all-atom force fields reported in literature, such as the one by Bourasseau et al. [5], the intermolecular interactions of NO_2 and N_2O_4 molecules are modeled using 3 parameters (σ and ϵ for the LJ interactions, and the point charge for the electrostatic interactions) for each atom type (N, O in either NO_2 or N_2O_4), leading to a total of 12 parameters. To reduce the computational cost of our simulations and simplify our system, we mapped both NO_2 and N_2O_4 molecules to single LJ particles with two interaction parameters (σ and ϵ). For LJ particles, T_c scales with the parameter ϵ ($T_c \sim \epsilon$) while the critical density scales with σ^3 ($\rho_c \sim \sigma^3$) [36]. To represent both NO_2 and N_2O_4 molecules as single LJ particles and adjust the σ and ϵ parameters for each molecule, we computed densities of pure NO_2 and pure N_2O_4 using single-component GE simulations (no reactions were included) and compared the computed densities as a function of temperature with the GEMC data from the study by Lasala et al. [21] for all-atom systems. To investigate possible finite-size effects, we also computed the densities of pure NO_2 and pure N_2O_4 as a function of the system size. Fig. 2 shows the comparison between densities computed by Lasala et al. [21] using Continuous Fractional Component Monte Carlo (CFCMC) simulations [37,63–66] and in this study by representing each molecule with a single LJ particle, as a function of temperature and system size. The force field parameters used in our simulations for NO_2 and N_2O_4 are shown in Table 1. Our results show an excellent agreement between the computed gas and liquid phase densities of pure NO_2 and those reported by Lasala et al. [21]. Fig. 2(b) shows that pure N_2O_4 gas phase densities are slightly overestimated at high temperatures, while the liquid phase densities are slightly underestimated at low temperatures. Overall, the computed densities of pure N_2O_4 are in good agreement with the results from Lasala et al. [21]. Also, Fig. 2 shows that finite-size effects on the densities computed using single-component GEMC simulations are very small. Fig. S1 of the Supplementary Material shows a comparison of the saturated vapor pressures as a function of temperature computed by Lasala et al. [21] using an all-atom force field, and computed here by representing NO_2 and N_2O_4 as single LJ particles. The vapor pressures of NO_2 computed using a single LJ site are in excellent agreement with the ones computed by Lasala et al. [21], while the vapor pressures of N_2O_4 are overestimated using a single LJ interaction site. This is expected since the computed densities of N_2O_4 do not agree with the results from Lasala et al. [21] computed using an all-atom force field as well as the computed densities of NO_2.

Table 1
Force field parameters, T_c, and ρ_c computed using single-component VLE of NO_2 (molar mass of NO_2, $M_{NO_2} = 46.0055\,g\,mol^{-1}$) and N_2O_4 ($M_{N_2O_4} = 92.011\,g\,mol^{-1}$). For T_c and ρ_c, the first values show the computed values in this work by using single LJ particles to represent NO_2 and N_2O_4 while the values in parentheses show the critical parameters computed by Lasala et al. [21]. Note that Lasala et al. [21] used all-atom force fields (with ϵ, σ, and point charge for each atom type) to perform Gibbs Ensemble simulations with the CFCMC [37,65,66] method. Note that the values of T_c and ρ_c are shown for pure NO_2 and pure N_2O_4 without considering reaction R1.

Particle	ϵ/k_B/[K]	σ/[Å]	T_c/[K]	ρ_c/[kg m⁻³]
NO_2	262.17	3.727	282.4 (282.2)	473.1 (471.8)
N_2O_4	445.00	4.450	484.5 (484.2)	546.3 (502.4)

Next, we computed the values of $\left(\frac{\rho_l-\rho_g}{\rho_0}\right)^{\frac{1}{\beta}}$ ($\beta = 0.32$) as a function of temperature for pure NO_2 and pure N_2O_4 (Eq. (1)). Fig. S2 of the Supplementary Material shows the values of the term $\left(\frac{\rho_l-\rho_g}{\rho_0}\right)^{\frac{1}{\beta}}$ for pure NO_2 and pure N_2O_4 as a function of temperature. The extrapolation of the line fitted to $\left(\frac{\rho_l-\rho_g}{\rho_0}\right)^{\frac{1}{\beta}}$ to zero as a function of temperature results in the critical temperature. Fig. S2 of the Supplementary Material shows the computed critical temperatures for pure NO_2 and pure N_2O_4 are 282.4 K and 484.5 K, respectively. In our previous study [21], we computed the critical temperatures of pure NO_2 and pure N_2O_4 as 282.2 K and 484.2 K, respectively, using CFCMC simulations [37,65,66]. This shows that the critical temperatures computed using a single LJ particle for each molecule are in excellent agreement with the critical temperatures computed using CFCMC simulations [21]. We also computed the average mass density of the gas and liquid phases as a function of temperature to compute ρ_c (mass-based) of pure NO_2 and pure N_2O_4 (Eq. (2)). Fig. S3 of the Supplementary Material shows the average mass density of the gas and liquid phases of pure NO_2 and pure N_2O_4 as a function of temperature. The extrapolation of the line fitted to average mass density of the gas and liquid phases to the critical temperature results in the critical mass density. Fig. S3 of the Supplementary Material shows that the computed critical mass densities of pure NO_2 and pure N_2O_4 are 473.1 kg m⁻³ and 546.3 kg m⁻³, respectively. The critical mass density computed using the single LJ particle approach for pure NO_2 is in excellent agreement with the critical mass density computed in our recent study using CFCMC simulations (471.8 kg m⁻³) [21]. For pure N_2O_4, the critical mass density computed using a single LJ particle to represent N_2O_4 (546.3 kg m⁻³) is overestimated when compared to the results in our recent study (502.4 kg m⁻³) [21]. This is because it is less accurate to represent a molecule such as N_2O_4 as a spherical particle due to its elongated shape. However, our results for pure NO_2 demonstrate the accuracy of this approach. In any case, the agreement between the computed VLEs and critical properties using single LJ particle approach for NO_2 and N_2O_4 and the ones using CFCMC simulations [21] is good enough for our purposes for this study, which is to investigate the effect of force field parameters (ϵ and σ) and reaction equilibrium on the scaling towards the critical point.

3.2. Effect of the force field parameters on the scaling towards the critical point in reactive mixtures

We used RE/GEMC simulations to compute the phase and reaction equilibrium in the NO_2/N_2O_4 system as a function of temperature. For this purpose, in all simulations in this subsection, we calculated the isolated molecule partition functions of NO_2 and N_2O_4 (see Eq. (9)) using the correlations reported in the study by Lasala et al. [21]. The correlation to compute the isolated molecule partition function of N_2O_4 is [21]:

$$\ln\left[\frac{q_{N_2O_4}}{\Lambda_{N_2O_4}^3 \rho_0}\right] = 228591.177 \times T^{-1} + 23.218 \, / \, [-] \tag{11}$$
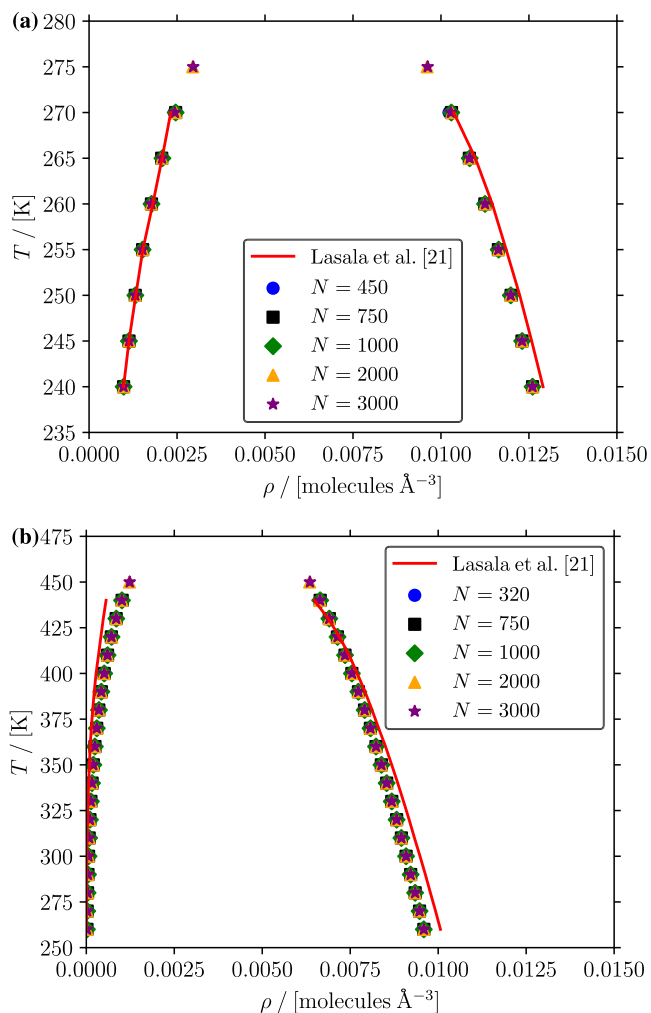
Fig. 2. Computed densities of (a) pure NO$_2$ and (b) pure N$_2$O$_4$ as a function of temperature and system size without considering reaction R1. The red lines represent results from Lasala et al. [21] computed using GEMC simulations while the symbols represent computed densities from this study using effective LJ particles (Table 1).

while for NO$_2$, the correlation to compute the isolated molecule partition function is [21]:

$$\ln\left[\frac{q_{NO_2}}{\Lambda_{NO_2}^3 \rho_0}\right] = 110983.613 \times T^{-1} + 16.403 \, / \, [-] \quad (12)$$

The values of isolated molecule partition functions as a function of temperature for NO$_2$ and N$_2$O$_4$ are listed in Table S1 of the Supplementary Material. We denote NO$_2$ and N$_2$O$_4$ by A and A$_2$, respectively, for force field parameters that are different from the listed in Table 1. To investigate the effect of the force field parameters on the scaling towards the critical point, we computed three sets of VLEs: (1) using the force field parameters listed in Table 1 ($\varepsilon_{N_2O_4}/\varepsilon_{NO_2} \approx 1.697$, $\sigma_{N_2O_4}/\sigma_{NO_2} \approx 1.194$), (2) using the same force field listed as N$_2$O$_4$ in Table 1 for A$_2$ except with ε_A/k_B as 187 K ($\varepsilon_{A_2}/\varepsilon_A \approx 2.380$, $\sigma_{A_2}/\sigma_A \approx 1.194$), and (3) using the same force field listed as N$_2$O$_4$ in Table 1 for A$_2$ except with σ_A as 3.423 Å ($\varepsilon_{A_2}/\varepsilon_A \approx 1.697$, $\sigma_{A_2}/\sigma_A \approx 1.300$). The parameters for different force fields used in our simulations are shown in Table 2. Table 3 lists the average pressures, chemical potentials of NO$_2$ and N$_2$O$_4$, and values of the terms $\sum_{i=1}^{S} \nu_i \mu_i$ for two simulation boxes in our RE/GEMC simulations using system 1 at 400 K. Our results show that the two simulation boxes are in mechanical and chemical equilibria as the pressures of the two simulation boxes are equal ($P^1 = P^2$), the chemical potentials of all species are equal in the two simulation boxes ($\mu_i^1 = \mu_i^2$), and Eq. (4)

holds for reaction R1 in both simulation boxes. Similar agreement is observed for all other simulations performed in this work. Fig. 3(a) shows the computed mole fractions of N$_2$O$_4$ in liquid (X_{dimer}) and gas (Y_{dimer}) phases as a function of temperature for the three different force field parameters for NO$_2$ (A). Our results show that the compositions of the mixture computed with different force field parameters for NO$_2$ are similar (except for the liquid phase at temperatures higher than 350 K). This shows that the reaction equilibrium of the NO$_2$/N$_2$O$_4$ system mainly depends on the value of isolated molecule partition functions (see Eq. (9)). To assess the applicability of the scaling law for the compositions towards the critical point as suggested by Wichterle et al. [44] (Eq. (3)), Fig. S4 of the Supplementary Material shows the values of the term $\left(X_i - Y_i\right)^{\frac{1}{\beta}}$ as a function of temperature for two different values of β and the coefficients of determination R^2 of the linear regression of the values of $\left(X_i - Y_i\right)^{\frac{1}{\beta}}$ as a function of β for the NO$_2$/N$_2$O$_4$ system. The results show that the values of the term $\left(X_i - Y_i\right)^{\frac{1}{\beta}}$ are not linear as a function of temperature for any value of β in the range of 0.1–1.5. This shows that the scaling law for the compositions as suggested by Wichterle et al. [44] is not applicable for reactive binary mixtures. As shown in Fig. 3(b), the densities computed with different force field parameters for NO$_2$ are also similar. For $\sigma_{NO_2} = 3.423$ Å ($\varepsilon_{A_2}/\varepsilon_A \approx 1.697$, $\sigma_{A_2}/\sigma_A \approx 1.300$, system 3), the liquid phase densities are higher than those of two other sets of force field parameters at temperatures higher than 350 K. We also compare the computed densities of the reactive NO$_2$/N$_2$O$_4$ mixture (system 1) with experimental liquid and gas densities from literature [67,68]. Fig. S5 of the Supplementary Material shows that the computed densities of the reactive mixture agree well with the experimental data [67,68] with a maximum deviation of 4%. Fig. S6 of the Supplementary Material shows a comparison of the computed densities of pure NO$_2$, pure N$_2$O$_4$, and the reactive mixture of NO$_2$ and N$_2$O$_4$ as a function of temperature. The computed densities of the liquid and gas phases of pure NO$_2$ are higher than those of pure N$_2$O$_4$ and the reactive binary mixture. At $T < 325$ K, the liquid and gas phase densities of pure N$_2$O$_4$ and the reactive mixture are similar, while at $T > 325$ K, the densities of the reactive binary mixture are slightly higher than those of pure N$_2$O$_4$ for both phases. This is expected since at $T < 325$ K, the reactive mixture is almost completely composed of N$_2$O$_4$ molecules (Fig. 3(a)). Also, we assessed possible finite-size effects on the compositions and densities of liquid and gas phases by performing RE/GEMC simulations with system 1 using three different total numbers of particles. Fig. 4 shows the compositions and densities of liquid and gas phases of system 1 (NO$_2$/N$_2$O$_4$ system) computed as a function of temperature and system size. Our data shows that the finite-size effects on both computed compositions and densities are insignificant in the combined RE/GEMC simulations.

Fig. 5(a) shows the values of $\left(\frac{\rho_l - \rho_g}{\rho_0}\right)^{\frac{1}{\beta}}$ as a function of temperature for $\beta = 0.32$ for three different sets of force field parameters and linear regression fits to these data sets. Our results show that linear regression fits are not very accurate ($R^2 = 0.98$) and the values of $\left(\frac{\rho_l - \rho_g}{\rho_0}\right)^{\frac{1}{\beta}}$ as a function temperature are not linear when $\beta = 0.32$ is used. This shows that for a LJ particle system with two components that acts like a single-component system because of the reaction R1, the value of β is different than 0.32 [36,38]. Fig. S7 of the Supplementary Material shows the values of R^2 of the linear regression of the values of $\left(\frac{\rho_l - \rho_g}{\rho_0}\right)^{\frac{1}{\beta}}$ as a function of β for three different force fields. Our results show that for systems 1 (the force field parameters listed in Table 1) and 3 (decreased σ_{NO_2}), the values of R^2 has a maxima at $\beta = 0.191_{0.02}$, while for system 2 (decreased ε_{NO_2}), the values of R^2 have a maxima at $\beta = 0.210_{0.02}$. However, for system 2, the value of R^2 is 0.999 at $\beta = 0.191$ and the differences between $R^2 = 1.0$ (a perfect linear regression fit) and $R^2 = 0.999$ is due to the statistical uncertainty in our simulations. Also, for system 2, the difference in critical temperatures computed using

Table 2

Force field parameters for monomers and dimers, values of the critical exponent β, computed values of T_c, and computed values of ρ_c for different systems investigated in this study. We denote NO_2 and N_2O_4 by A and A_2, respectively, for force field parameters that are different from the ones listed in Table 1 (this applies for systems 2, 3, 4, 5, and 6.). The force field parameters for systems 1, 4, 5, and 6 are same, but these systems differ in the values of isolated molecule partition functions of dimers (Tables S1-S4 of the Supplementary Material). The subscripts show the errors in the critical exponent β. The errors in the critical exponent β are computed based on maximum 1% deviation in the computed values of T_c. The average densities of the liquid and gas phases to compute the values of ρ_c (Eq. (2)) are calculated by summing the densities of monomer with twice the density of dimer as this corresponds to mass-based densities.

Sys.	$\frac{\varepsilon_{A_2}}{\varepsilon_A}$	$\frac{\sigma_{A_2}}{\sigma_A}$	Dimer		Monomer		β	T_c/[K]	ρ_c/[molecules Å^{-3}]
			ε/k_B/[K]	σ/[Å]	ε/k_B/[K]	σ/[Å]			
1	1.697	1.194	445.00	4.450	262.17	3.727	$0.191_{0.02}$	417	0.00767
2	2.380	1.194	445.00	4.450	187.00	3.727	$0.210_{0.02}$	416	0.00798
3	1.697	1.300	445.00	4.450	262.17	3.423	$0.191_{0.01}$	425	0.00787
4	1.697	1.194	445.00	4.450	262.17	3.727	$0.299_{0.01}$	300	0.00915
5	1.697	1.194	445.00	4.450	262.17	3.727	$0.270_{0.01}$	464	0.00733
6	1.697	1.194	445.00	4.450	262.17	3.727	$0.259_{0.01}$	302	0.01024

Table 3

Average pressures, chemical potentials of NO_2 and N_2O_4 (Eq. (5)), and values of the terms $\sum_{i=1}^{S} \nu_i \mu_i$ (Eq. (4)) for two simulation boxes in our RE/GEMC simulations (including reaction R1) for system 1 at 400 K. The subscripts show the standard deviations computed using the results of ten independent simulations.

	Box 1	Box 2
P/[kPa]	5495_{12}	5494_{10}
μ_{NO_2}/[kJ mol^{-1}]	$-1003.011_{0.004}$	$-1003.012_{0.003}$
$\mu_{N_2O_4}$/[kJ mol^{-1}]	$-2006.024_{0.005}$	$-2006.027_{0.006}$
$\sum_{i=1}^{S} \nu_i \mu_i$/[kJ mol^{-1}]	$0.001_{0.003}$	$0.002_{0.001}$

$\beta = 0.210$ and $\beta = 0.191$ is lower than 1% (as shown in Table 2 by the errors in the estimate of β). This shows that the values of β do not depend on force field parameters of LJ particles.

Fig. 5 shows the values of the term $\left(\frac{\rho_l - \rho_g}{\rho_0}\right)^{\frac{1}{\beta}}$ for $\beta = 0.32$ (Fig. 5(a)) and $\beta = 0.191$ (Fig. 5(b)) as a function of temperature for varying force field parameters. By extrapolating the linear regression fits of $\left(\frac{\rho_l - \rho_g}{\rho_0}\right)^{\frac{1}{\beta}}$ to zero, we compute the critical temperatures for different mixtures of NO_2 and N_2O_4. For $\beta = 0.32$, we compute the critical temperature of the mixture computed using the force field parameters listed in Table 1 (system 1) as 453 K while the critical temperature is 417 K for the same mixture for $\beta = 0.191$. The experimental critical temperature for NO_2/N_2O_4 system reported in literature [69] is 431 K. Our results show that our approach in computing phase and reaction equilibrium using single LJ particles for molecules is accurate, however, parameterization of the critical exponent β is essential for accurate computation of critical temperatures of binary mixtures which act as a single-component system due to a chemical reaction.

Fig. 6 shows average mass and number densities between liquid and gas phases computed using different force fields as listed in Table 2. Eq. (2) implies that average densities of the liquid and gas phases should scale linearly with temperature. Fig. 6 shows that the average mass densities of a NO_2/N_2O_4 system scale linearly with temperature, while the average number densities do not (see Fig. S8 of the Supplementary Material). Our results show that average mass densities (or number densities where the density of the dimer is counted twice) needs to be used to compute critical densities using Eq. (2). By extrapolating the linear regression fits of average mass densities of liquid and gas phases computed using the force field parameters listed in Table 1 (system 1) to the critical temperature computed using Fig. 5 and $\beta = 0.191$ (Fig. 6(a)), we compute the critical density of NO_2/N_2O_4 system as 585.8 kg m^{-3}, showing an excellent agreement with the experimental value [69] (560 kg m^{-3}). This shows that representing fully atomistic models of NO_2 and N_2O_4 as single LJ particles is accurate enough for computing critical densities using RE/GEMC simulations.
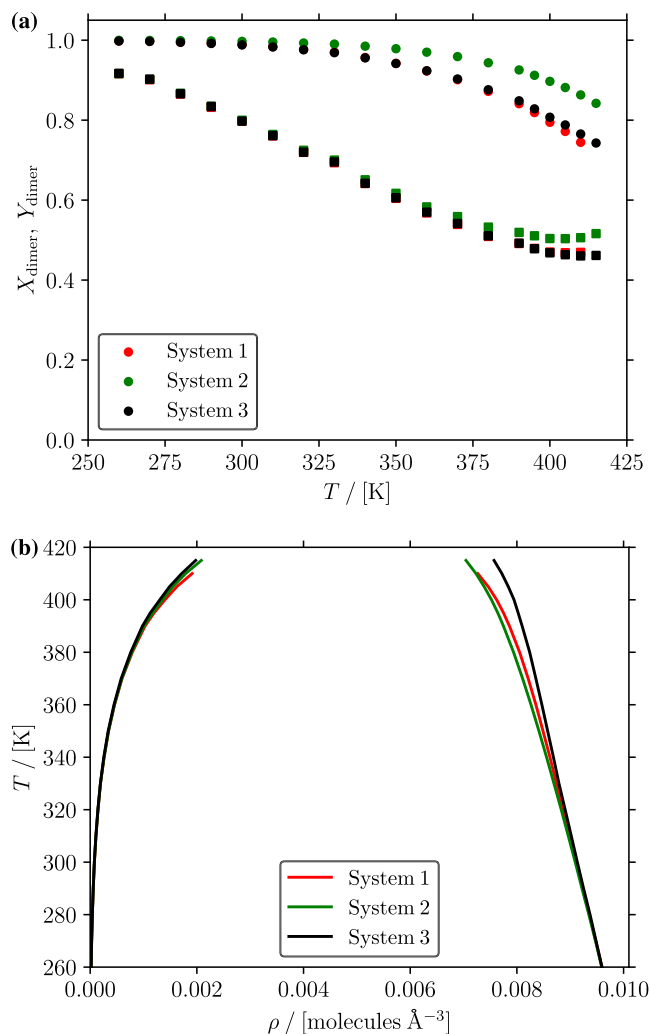

Fig. 3. (a) Mole fractions of dimer molecules (N_2O_4 or A_2) in liquid (circles) and gas (squares) phases and (b) coexistence densities computed using different force field parameters for NO_2 and considering reaction R1. See Table 2 for the force field parameters used in systems 1, 2, and 3.

3.3. Effect of the isolated molecule partition functions on the scaling towards the critical point

We performed RE/GEMC simulations to compute phase and reaction equilibria as a function of temperature and varying the isolated molecule partition function of N_2O_4. We denote NO_2 and N_2O_4 by A and A_2, respectively, for isolated molecule partition functions that
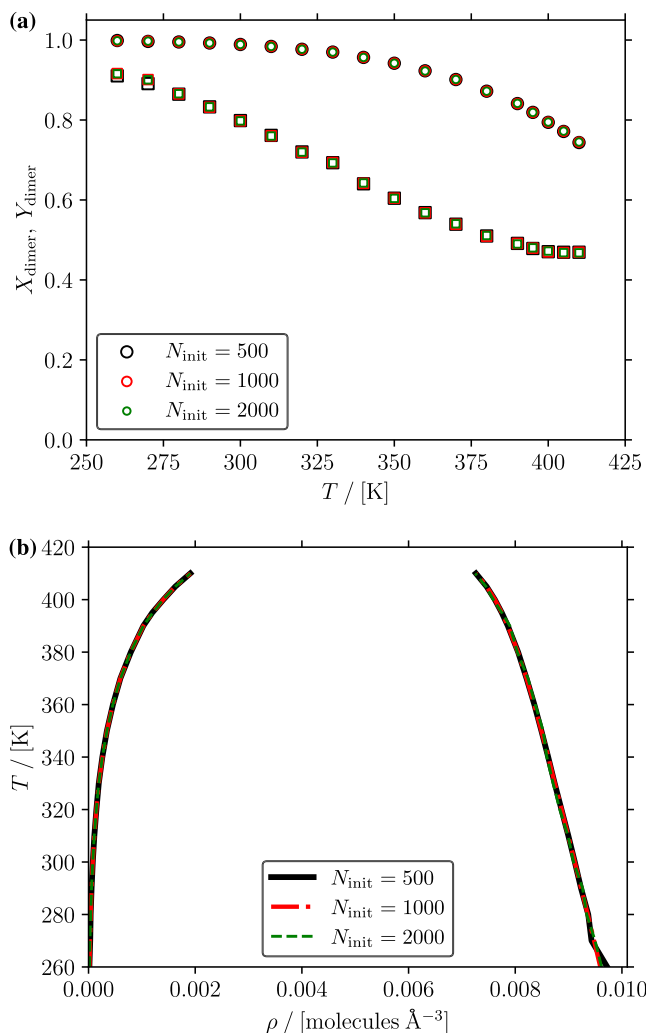
(a)

(b)

Fig. 4. (a) Mole fractions of dimer molecules in liquid (circles) and gas (squares) phases and (b) coexistence densities computed considering reaction R1 as a function of temperature and different initial system sizes. To assess the finite-size effects on the compositions and densities computed using RE/GEMC simulations, we used force field parameters of system 1 as listed in Table 2.

(a)

(b)

Fig. 5. Values of $\left(\frac{\rho_l - \rho_g}{\rho_0}\right)^{\frac{1}{\beta}}$ for (a) $\beta = 0.32$ and (b) $\beta = 0.191$ as a function of temperature for mixtures with different force field parameters. NO_2 and N_2O_4 (which have different force field parameters than the ones listed in Table 1) are denoted by A and A_2, respectively. We computed the values of ρ_l and ρ_g as a function of temperature by using RE/GEMC simulations (with reaction R1). To compute the values of $\left(\frac{\rho_l - \rho_g}{\rho_0}\right)^{\frac{1}{\beta}}$, we used number densities. The dashed lines represent linear regression fits to the values of $\left(\frac{\rho_l - \rho_g}{\rho_0}\right)^{\frac{1}{\beta}}$ as a function of temperature. See Table 2 for the force field parameters used in systems 1, 2, and 3.

are different from the ones computed using the correlations reported by Lasala et al. [21] (system 1). Our simulations used the force field parameters from Table 1 for both NO_2 (A) and N_2O_4 (A_2) to calculate LJ interactions (also listed in Table 2). Fig. 7(a) shows the natural logarithm of isolated molecule partition functions for NO_2 (A) and N_2O_4 (A_2) used in our simulations as a function of temperature. Different values of natural logarithm of isolated molecule partition functions for monomers and dimers are listed in Tables S1-S4 of the Supplementary Material. Our data reveal that even small modifications to the isolated molecule partition function of A_2 result in very different reaction equilibrium constants. We recently discovered that the computed reaction equilibrium constants for the dissociation of protonated *N*-methyldiethanolamine are also very sensitive to the values of isolated molecule partition functions or excess chemical potentials [56]. Fig. 7(b) shows the natural logarithm of reaction equilibrium constants for reaction R1 computed as a function of inverse temperature using different values of isolated molecule partition functions and Eq. (10). The computed ideal gas equilibrium constants for reaction R1 show that even with small changes in the values of isolated molecule partition function of species, the reaction equilibrium is completely different. For example, natural logarithms of reaction equilibrium constants computed using the isolated molecule partition
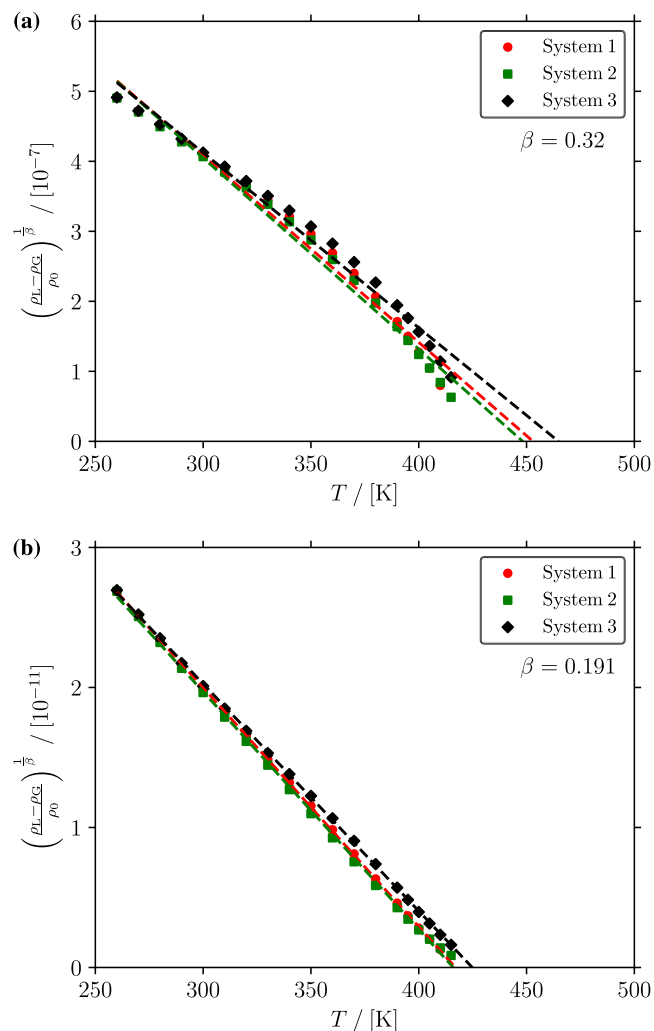
functions from Lasala et al. [21] (Eqs. (11) and (12)) are in the range of 6.4–15.8 for temperatures of 260–415 K while using slightly decreased values of isolated molecule partition functions for A_2 (decreased by 10 ln $\left[\frac{q_i}{\Lambda_i^3 \rho_0}\right]$ units for each temperature, system 4), the natural logarithms of reaction equilibrium constants are −3.6–5.8 for the same temperature range. We also compute the ideal gas enthalpies of reaction for these systems using the Van't Hoff equation [60]:

$$\frac{d \ln[K_{\text{IG}}]}{dT} = \frac{-\Delta_r H}{RT^2} \tag{13}$$

where $\Delta_r H$ is ideal gas enthalpy of reaction and R is the ideal gas constant. While reaction equilibrium constants computed using the isolated molecule partition functions from Lasala et al. [21] (system 1) and reaction equilibrium constants computed using slightly decreased values of isolated molecule partition functions for A_2 (system 4) have the same values of $\Delta_r H$ (−55.08 kJ mol^{-1}), the values of $\Delta_r H$ for the reaction equilibrium constants computed using the values of ideal
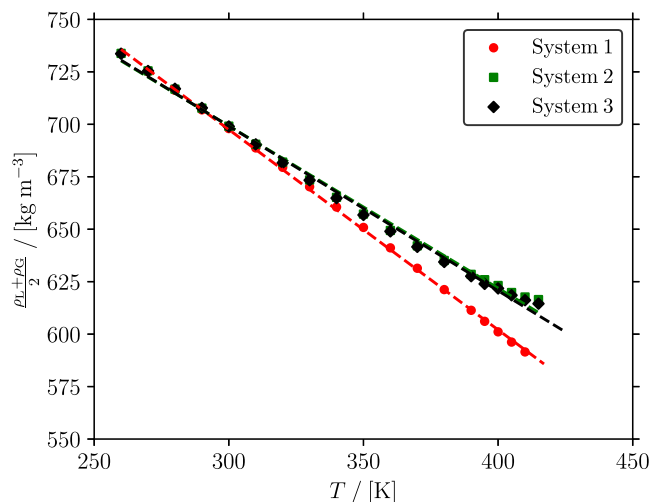
Fig. 6. Average mass densities of the liquid and gas phases computed using different force fields as shown in Table 2 with reaction R1. The dashed lines represent linear regression fits to average mass densities computed as a function of temperature using different force fields. See Table 2 for the force field parameters used in systems 1, 2, and 3.

partition functions of N_2O_4 increased by 1% and decreased by 1% for each temperature point (systems 5 and 6, respectively) are different ($-74.08 \, \text{kJ} \, \text{mol}^{-1}$ and $-36.07 \, \text{kJ} \, \text{mol}^{-1}$, respectively).

Fig. S8(a) of the Supplementary Material shows mole fractions of dimers in the liquid and gas phases computed for different values of the isolated molecule partition function for A_2 as a function of temperature. Our results show that the compositions of gas and liquid phases of the reactive binary mixtures are very sensitive to the values of the equilibrium constant of reaction R1. Also, it can be observed that both gas and liquid phases are predominantly composed of dimers even at high temperatures when the isolated molecule partition functions of system 5 are used as opposed to mole fractions computed using system 1 where mole fractions of dimer in the liquid and gas phases are 0.74 and 0.47, respectively, at 410 K. When the isolated molecule partition functions of systems 4 and 6 are used in our RE/GEMC simulations, the computed compositions of liquid and gas phases are very different than the compositions computed using systems 1 and 5. At 260 K, the mole fractions of dimers in liquid phase are 0.73 and 0.78 when systems 4 and 6 are considered, respectively. At the same temperature, the liquid phases are almost fully composed of dimer molecules when systems 1 and 5 are simulated. Fig. S9(b) of the Supplementary Material shows the densities of gas and liquid phases computed as a function of temperature using different values of isolated molecule partition functions for A_2. Our data show that the liquid phase densities are similar for systems 1 and 5. The gas phase densities are much lower at high temperatures when system 5 is used compared to when the ideal partition functions of system 1 are used. The gas phase densities computed using systems 4 and 6 are similar and are higher than those computed using systems 1 and 5. When isolated molecule partition functions of system 6 are used, the computed densities of the liquid phase are higher than the ones computed using systems 1, 4, and 5.

Next, we investigate the effect of reaction equilibrium on the scaling towards the critical point. For this purpose, we use linear regression fits to the values of the term $\left(\frac{\rho_l - \rho_g}{\rho_0} \right)^{\frac{1}{\beta}}$ as a function of temperature. We first computed the values of R^2 of the linear regression fits to the values of the term $\left(\frac{\rho_l - \rho_g}{\rho_0} \right)^{\frac{1}{\beta}}$ vs. temperature as a function of the critical exponent β. Fig. S10 of the Supplementary Material shows that when the parameter set of system 5 is used, the values of R^2 has a maxima at $\beta = 0.270_{0.01}$ (subscripts indicate the error in β when accounting
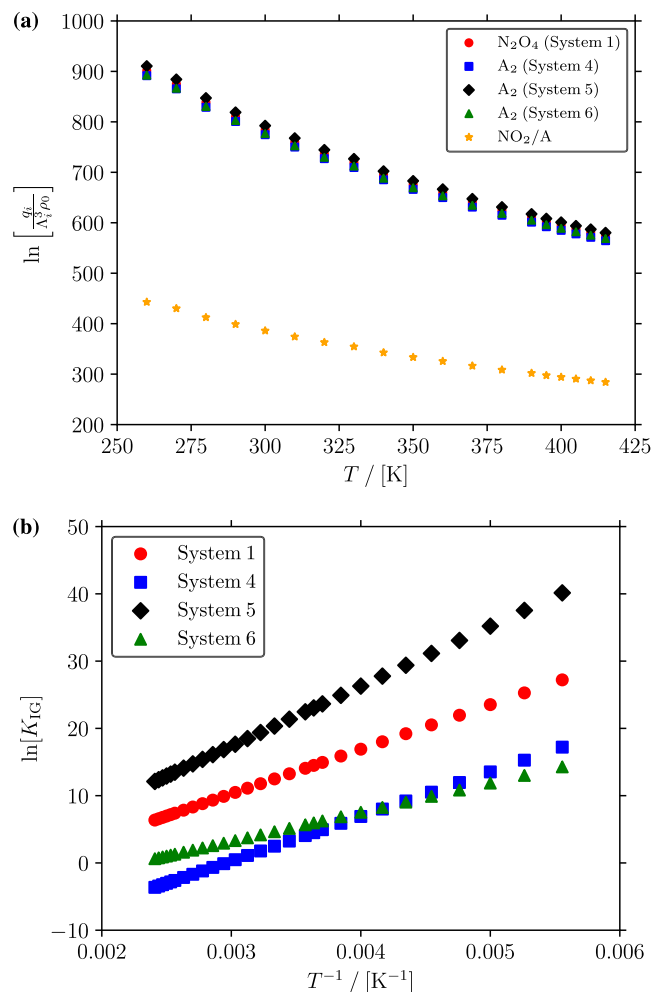

Fig. 7. (a) Natural logarithm of the values of isolated molecule partition functions as a function of temperature used in our RE/GEMC simulations and (b) natural logarithm of ideal gas equilibrium constants (Eq. (10)) for reaction R1 as a function of inverse temperature. See Table 2 for the force field parameters and Tables S1-S4 of the Supplementary Material for the values of isolated molecule partition functions of monomers and dimers for different systems.

for 1% deviation in the computed values of T_c) which is different than the maxima when the ideal partition functions are computed using the correlations reported by Lasala et al. [21] (for system 1, $\beta = 0.191_{0.02}$). For systems 4 and 6, the maxima of R^2 are at $\beta = 0.299_{0.01}$ and $\beta = 0.259_{0.01}$, respectively. However, for higher values of β, R^2 for systems 4 and 6 are higher than 0.995, showing that the values of R^2 for these systems are less sensitive than the respective R^2 for systems 1 and 5. Our results indicate that β varies for systems with different reaction equilibrium constants, associated with different enthalpies of reaction.

Fig. 8(a) shows the values of R^2 for linear regression fits to $\left(\frac{\rho_l - \rho_g}{\rho_0} \right)^{\frac{1}{\beta}}$ as a function of β for system 1. Our data show that the values of β between 0.141 and 0.277 have R^2 values higher than 0.99. However, as shown in Fig. 8(b) and (d), the scaling of densities of liquid and gas phases are not linear when $\beta = 0.141$ and $\beta = 0.277$. Using $\beta = 0.141$ and $\beta = 0.277$, the computed values of T_c for system 1 are 404 K and 441 K, respectively. This shows that even with $R^2 = 0.99$, there is significant error in the computed T_c when compared with T_c computed using the value of the critical exponent as 0.191 (417 K with $\beta = 0.191$ as shown in Fig. 8(c)). The estimates of β as listed in Table 2 correspond to $R^2 > 0.9995$. A deviation of 1% in the values of T_c correspond to ca. $R^2 = 0.999$. Our findings demonstrate that varying reaction equilibria
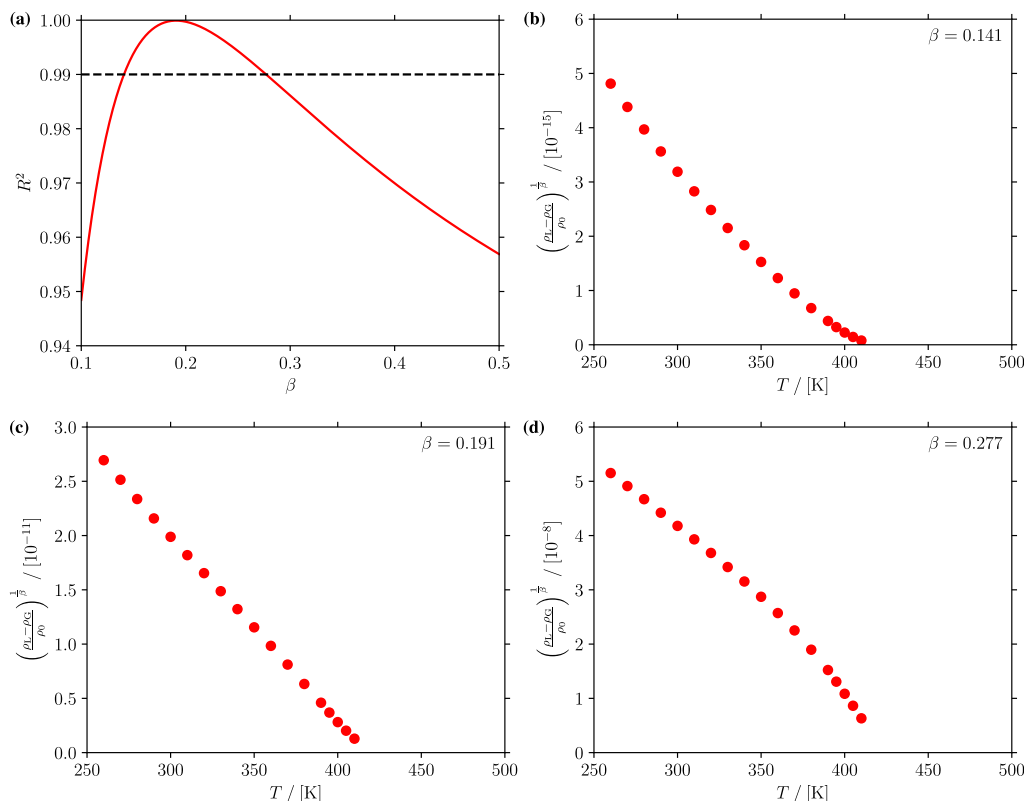
Fig. 8. (a) Coefficients of determination for linear regression fits to the terms $\left(\frac{\rho_l - \rho_g}{\rho_0}\right)^{\frac{1}{\beta}}$ as a function of temperature, and values of the terms $\left(\frac{\rho_l - \rho_g}{\rho_0}\right)^{\frac{1}{\beta}}$ as a function of temperature for (b) $\beta = 0.141$, (c) $\beta = 0.191$, and (d) $\beta = 0.277$ for system 1. The dashed line in subfigure (a) represents $R^2 = 0.99$. An uncertainty of 1% in the values of T_c corresponds to ca. $R^2 = 0.999$. See Table 2 for the force field parameters and Table S1 of the Supplementary Material for the values of isolated molecule partition functions of monomers and dimers for system 1.

has a strong impact on the scaling behavior towards the critical point in systems with two components, albeit behaving like a single-component system due to a chemical reaction. Thus, careful parameterization of the critical exponent β is essential for accurate computation of critical temperatures and densities.

3.4. Screening the critical exponent β, T_c, and ρ_c for different values of K_{IG}

In the gas phase, there are many examples of monomers forming dimers such as aluminum chloride ($2AlCl_3 \rightleftharpoons Al_2Cl_6$) [1,46] and aluminum bromide ($2AlBr_3 \rightleftharpoons Al_2Br_6$) [46,47]. However, the thermodynamics and kinetics of dimerization of different monomer/dimer pairs are largely unknown. Due to lack of available thermodynamic data, we perform a screening study to investigate how the values of β, T_c, and ρ_c change for ideal gas reaction equilibrium constants K_{IG} with different temperature dependencies assuming a fast dimerization equilibrium reaction. For this purpose, we use force field parameters for monomers and dimers in reduced units. We select $\frac{\sigma_{dimer}}{\sigma_{monomer}}$ as 1.194 based on the fact that the volume of the dimer is ca. double that of monomer, which scales with σ^3 ($1.194^3 \approx 2$). The number of atoms in a dimer is twice that of a monomer, however the chemical environment is different between a monomer and a dimer. To account for this difference, we choose $\frac{\varepsilon_{dimer}}{\varepsilon_{monomer}}$ as 1.697. This choice ensures that the LJ interactions between monomers and dimers appropriately capture size and energy differences. Earlier, we showed that these force field parameters accurately describe the VLEs of pure monomer (NO_2) and pure dimer (N_2O_4, Section 3.1). We describe the temperature dependence of the values of K_{IG} using an Arrhenius type equation [60]:

$$K_{IG} = K_0 \exp\left[\frac{-\Delta_r H}{RT}\right] \tag{14}$$

where K_0 is the pre-exponential factor associated with the ideal gas reaction equilibrium constant at infinite temperature. We then vary the values of the natural logarithm of K_0 ($\ln[K_0]$) and the dimensionless enthalpy of reaction ($\Delta_r^* H$) which is calculated as:

$$\Delta_r^* H = \frac{\Delta_r H}{RT_{c,monomer}} \tag{15}$$

where $T_{c,monomer}$ is the critical temperature of pure monomer (282.4 K, Table 1). We compute the values of the critical exponent β, the normalized T_c ($T_c^* = T_{c,mixture}/T_{c,monomer}$ where $T_{c,mixture}$ is the critical temperature of the reactive binary mixture), and the normalized ρ_c ($\rho_c^* = \rho_{c,mixture}/\rho_{c,monomer}$ where $\rho_{c,mixture}$ and $\rho_{c,monomer}$ are the critical densities of the reactive binary mixture and pure monomer, respectively) for systems with different values of $\ln[K_0]$ (ranging from -19.6 to 0.4) different values of $\Delta_r^* H$ (ranging from -36 to -17) using RE/GEMC simulations. Tables S5–S7 of the Supplementary Material lists the values of β, T_c^*, and ρ_c^* as a function of $\Delta_r^* H$ and $\ln[K_0]$. Fig. 9(a) shows the computed values of β as a function of the values of $\ln[K_0]$ and $\Delta_r^* H$. The computed values of β vary from 0.124 to 0.282 which shows that a parameterization of β is crucial for an accurate estimation of T_c. Our data show that β decreases with increasing $\Delta_r^* H$, while β increases with increasing $\ln[K_0]$. Fig. 9(b) shows the values of T_c^* as a function of $\Delta_r^* H$ and $\ln[K_0]$. T_c^* is proportional to $\ln[K_0]$, and decreases with increasing $\Delta_r^* H$, varying between 1.28–1.67 times $T_{c,monomer}$. Fig. 9(c) shows ρ_c^* as a function of $\Delta_r^* H$ and $\ln[K_0]$. Note that the average densities of the liquid and gas phases are calculated by summing the densities of monomer with twice the density of dimer as this corresponds to mass-based densities. We already showed that mass-based average densities scale better than number-based average densities towards the critical point (Fig. 6 and Fig. S8 of the Supplementary Material). The values of ρ_c^* show a different trend than the values of β and T_c^*. The computed ρ_c^* decrease with increasing $\ln[K_0]$, and increase with increasing $\Delta_r^* H$.
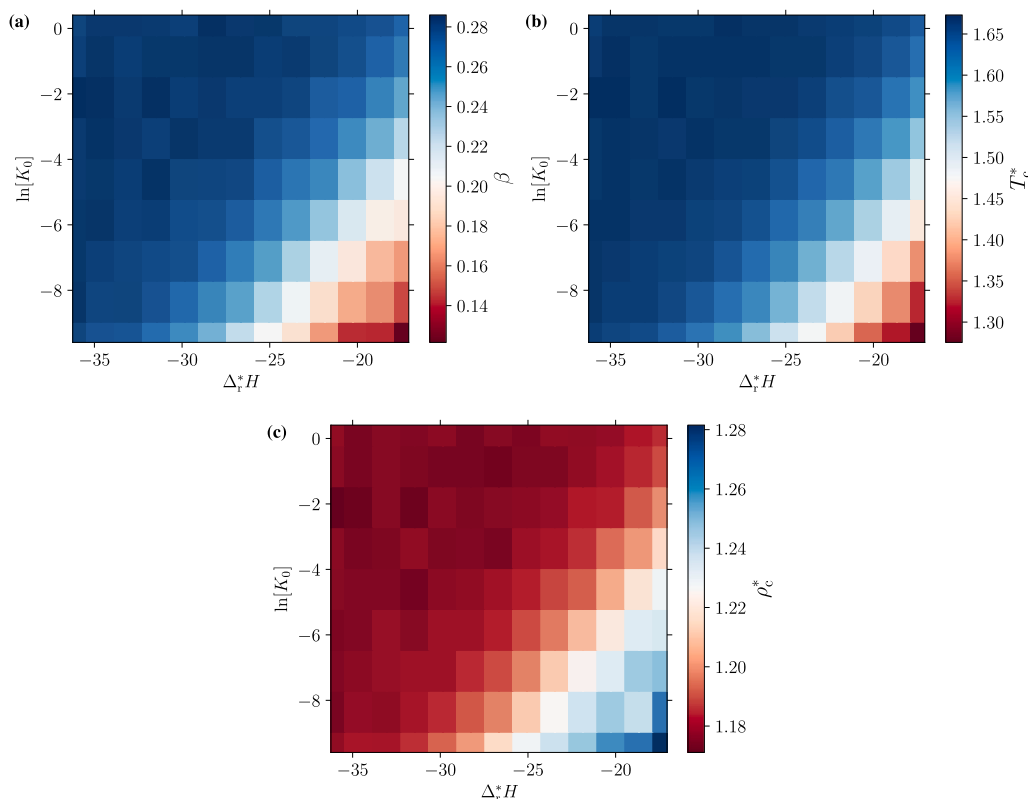
Fig. 9. Values of (a) β, (b) T_c^*, and (c) ρ_c^* of reactive binary mixtures as a function of natural logarithms of pre-exponential factors ($\ln[K_0]$, Eq. (14)) and dimensionless enthalpies of reaction ($\Delta_r^* H$, Eq. (15)). For all systems, the linear regression fits to $\left(\frac{\rho_l - \rho_g}{\rho_0}\right)^{\frac{1}{\beta}}$ and $\frac{\rho_l + \rho_g}{2}$ as a function of temperature resulted in $R^2 > 0.999$.

ρ_c^* vary between 1.17–1.28 times $\rho_{c,monomer}$. We show that if the ideal gas reaction equilibrium constant favors dimerization (lower values of $\Delta_r^* H$ and higher values of $\ln[K_0]$), the scaling towards the critical point is slower (the densities of the liquid and gas phases approach to critical density less rapidly as the temperature increases due to higher values of β), the critical temperature is higher, and consequently the critical density is lower. The values of the critical exponent β, T_c^*, and ρ_c^* for different monomer/dimer pairs, obtained using RE/GEMC simulations, can serve as a predictive tool for assessing the critical point of reactive binary mixtures. This predictive capability enhances the efficiency of screening processes, enabling the identification of optimal conditions for specific monomer/dimer combinations in diverse scientific and engineering applications.

4. Conclusions

We investigated the effect of force field parameters and isolated molecule partition functions on the scaling towards the critical point of reactive binary mixtures, which exhibit similar phase characteristics to that of a single-component system due to a fast dimerization reaction. To simplify our simulations and minimize the computational cost, both NO_2 (monomer) and N_2O_4 (dimer) molecules were represented by single LJ interaction sites with carefully fine-tuned force field parameters. The computed liquid and gas phase densities of pure (unreactive) NO_2 and N_2O_4 showed an excellent agreement with densities computed using an all-atom force field [21]. Using RE/GEMC simulations, we established that a critical exponent of $\beta = 0.191$ is necessary for an accurate estimation of the value of T_c of the reactive NO_2/N_2O_4 mixture. The critical exponent $\beta = 0.191$ remained constant, regardless of changes in the force field parameters (σ and ϵ) of monomers. Our findings demonstrated that changes in isolated molecule partition functions of dimers have a significant impact on β. We showed that the value of β differs from 0.124 to 0.282, decreasing with increasing

$\Delta_r^* H$, and increasing with increasing $\ln[K_0]$ (Eq. (14)). The computed values of β for ideal gas reaction equilibrium constants with different temperature dependencies enable accurate estimations of the values of T_c and ρ_c for different monomer/dimer pairs.

We performed a screening of normalized values of T_c (T_c^*) and observed a similar trend as with β, where T_c^* increases with decreasing values of $\Delta_r^* H$ and increases with higher $\ln[K_0]$. This is because lower values of β lead to faster scaling towards the critical point (the densities of the liquid and gas phases approach critical density rapidly as the temperature increases) and consequently the critical temperature is lower. The values of T_c^* were computed to be 1.28–1.67 times higher than the T_c of monomer. We showed that the normalized values of ρ_c (ρ_c^*) increases with higher values of $\Delta_r^* H$ and decreases with increasing $\ln[K_0]$, varying between 1.17–1.28 times that of the monomer. Our study emphasizes the significance of accurate parameterization of β in capturing the scaling towards the critical point accurately. These findings are very important for a wide range of scientific and engineering applications where accurate modeling of phase behavior is essential. Present approach allows us to compute the values of T_c and ρ_c for reactive binary mixtures, but not the composition of the mixture at the critical point because, to the best of our knowledge, there are no scaling laws describing the scaling of composition towards the critical point in reactive mixtures. In this context, multiple histogram reweighting combined with grand-canonical Monte Carlo simulations has the potential to provide valuable insight into how the compositions of reactive binary mixtures scale towards the critical point as this method offers higher accuracies close to the critical point [30–36].

CRediT authorship contribution statement

H. Mert Polat: Writing – review & editing, Writing – original draft, Software, Methodology, Investigation. **Silvia Lasala:** Writing – review & editing, Validation, Supervision, Methodology, Investigation,

Conceptualization. **Frédérick de Meyer:** Writing – review & editing, Supervision, Methodology, Conceptualization. **Céline Houriez:** Writing – review & editing, Supervision, Methodology, Conceptualization. **Othonas A. Moultos:** Writing – review & editing, Supervision, Methodology, Formal analysis, Conceptualization. **Thijs J.H. Vlugt:** Writing – review & editing, Validation, Supervision, Software, Resources, Methodology, Funding acquisition, Conceptualization.

Declaration of competing interest

The authors declare that they have no known competing financial interests or personal relationships that could have appeared to influence the work reported in this paper.

Data and software availability

The in-house code for RE/GEMC simulations with example input files can be downloaded from https://doi.org/10.4121/a3ecbf66-624a-4dde-ae50-de951bc2a069.v1.

Data and software availability

The in-house code for RE/GEMC simulations with example input files can be downloaded from https://doi.org/10.4121/a3ecbf66-624a-4dde-ae50-de951bc2a069.v1.

Appendix A. Supplementary data

Supplementary material related to this article can be found online at https://doi.org/10.1016/j.fluid.2024.114084.

References

[1] M. Blander, L.G. Epel, A.P. Fraas, R.F. Newton, Aluminum Chloride As a Thermodynamic Working Fluid and Heat Transfer Medium, Tech. rep., Oak Ridge National Lab. (ORNL), ORNL-2677, 1959, Accessed on 24/10/2023. URL http://dx.doi.org/10.2172/4209651.

[2] A. Treinin, E. Hayon, Absorption spectra and reaction kinetics of NO_2, N_2O_3, and N_2O_4 in aqueous solution, J. Am. Chem. Soc. 92 (1970) 5821–5828.

[3] K. Kesavan, The Use of Dissociating Gases As the Working Fluid in Thermodynamic Power Conversion Cycles (PhD thesis), Carnegie-Mellon University, Pittsburgh, Pennsylvania, 1978, URL https://www.proquest.com/openview/c0920507f648498a5b1c8afcabf69ede.

[4] M.S. Jetten, M. Schmid, I. Schmidt, M. Wubben, U. van Dongen, W. Abma, O. Sliekers, N.P. Revsbech, H.J. Beaumont, L. Ottosen, E. Volcke, H. Laanbroek, J.L. Campos-Gomez, J. Cole, M. van Loosdrecht, J.W. Mulder, J. Fuerst, D. Richardson, K. van de Pas, R. Mendez-Pampin, K. Third, I. Cirpus, R. van Spanning, A. Bollmann, L.P. Nielsen, H.O. den Camp, C. Schultz, J. Gundersen, P. Vanrolleghem, M. Strous, M. Wagner, J.G. Kuenen, Improved nitrogen removal by application of new nitrogen-cycle bacteria, Rev. Environ. Sci. Bio/Technol. 1 (2002) 51–63.

[5] E. Bourasseau, V. Lachet, N. Desbiens, J.-B. Maillet, J.-M. Teuler, P. Ungerer, Thermodynamic behavior of the CO_2 + NO_2/N_2O_4 mixture: A Monte Carlo simulation study, J. Phys. Chem. B 112 (2008) 15783–15792.

[6] A. Belkadi, F. Llovell, V. Gerbaud, L. Vega, Modeling the vapor–liquid equilibrium and association of nitrogen dioxide/dinitrogen tetroxide and its mixtures with carbon dioxide, Fluid Phase Equilib. 266 (2008) 154–163.

[7] M. Shiri, M.A. Zolfigol, H.G. Kruger, Z. Tanbakouchian, Advances in the application of N_2O_4/NO_2 in organic reactions, Tetrahedron 66 (2010) 9077–9106.

[8] E. Neyrolles, A. Valtz, C. Coquelet, A. Chapoy, On the phase behaviour of the CO_2 + N_2O_4 system at low temperatures, Chem. Eng. Sci. 258 (2022) 117726.

[9] D.W. James, R.C. Marshall, Electron spin resonance study of the dinitrogen tetroxide-nitrogen dioxide system, J. Phys. Chem. 72 (1968) 2963–2966.

[10] R. Stochl, Potential Performance Improvement using a Reacting Gas (Nitrogen Tetroxide) As the Working Fluid in a Closed Brayton Cycle, Tech. rep., National Aeronautics and Space Administration (NASA), NASA-TM-79322, 1979, Accessed on 24/10/2023. URL https://ntrs.nasa.gov/api/citations/19800008230/downloads/19800008230.pdf.

[11] A. Sorokin, Dissociating nitrogen tetroxide (N_2O_4) as a working fluid in thermodynamic cycles, Nucl. Sci. Eng. 72 (1979) 330–346.

[12] H.M. Huang, R. Govind, Use of dissociating gases in brayton cycle space power systems, Ind. Eng. Chem. Res. 27 (1988) 803–810.

[13] S. Lasala, R. Privat, O. Herbinet, P. Arpentinier, D. Bonalumi, J.-N. Jaubert, Thermo-chemical engines: Unexploited high-potential energy converters, Energy Convers. Manage. 229 (2021) 113685.

[14] A. Barakat, S. Lasala, P. Arpentinier, J.-N. Jaubert, The original and impactful exploitation of chemical energy in heat pumps, Chem. Eng. J. Adv. 12 (2022) 100400.

[15] R.R. Furgason, J.M. Smith, Enthalpy and heat capacity of N_2O_4-NO_2 at pressure above one atmosphere, J. Chem. Eng. Data 7 (1962) 528–529.

[16] W.S. Hines, W.H. Nurick, High Performance of N_2O_4/Amine Elements, Tech. rep., National Aeronautics and Space Administration (NASA), NASA-CR-147555, 1974, Accessed on 24/10/2023. URL https://ntrs.nasa.gov/api/citations/19760015308/downloads/19760015308.pdf.

[17] I. Frank, A. Hammerl, T.M. Klapötke, C. Nonnenberg, H. Zewen, Processes during the hypergolic ignition between monomethylhydrazine (MMH) and dinitrogen tetroxide (N_2O_4) in rocket engines, Propellants, Explos. Pyrotech. 30 (2005) 44–52.

[18] P.K. Mueller, M. Hitchcock, Air quality criteria—toxicological appraisal for oxidants, nitrogen oxides, and hydrocarbons, J. Air Pollut. Control Assoc. 19 (1969) 677–678.

[19] S. Camy, J.-J. Letourneau, J.-S. Condoret, Experimental study of high pressure phase equilibrium of (CO_2+NO_2/N_2O_4) mixtures, J. Chem. Thermodyn. 43 (2011) 1954–1960.

[20] L.E.S. de Souza, U.K. Deiters, Modeling of the N_2O_4–NO_2 reacting system, Phys. Chem. Chem. Phys. 2 (2000) 5606–5613.

[21] S. Lasala, K. Samukov, H.M. Polat, V. Lachet, O. Herbinet, R. Privat, J.-N. Jaubert, O.A. Moultos, K.D. Ras, T.J.H. Vlugt, Application of thermodynamics at different scales to describe the behaviour of fast reacting binary mixtures in vapour-liquid equilibrium, Chem. Eng. J. 483 (2024) 148961.

[22] J.C. Conklin, G.E. Courville, J.H. Scott, Evaluation of active working fluids for brayton cycles in space applications, AIP Conf. Proc. 699 (2004) 463–472.

[23] J.K. Johnson, A.Z. Panagiotopoulos, K.E. Gubbins, Reactive canonical Monte Carlo, Mol. Phys. 81 (1994) 717–733.

[24] S. Lasala, P. Chiesa, R. Privat, J.-N. Jaubert, VLE properties of CO_2 – based binary systems containing N_2, O_2 and Ar: Experimental measurements and modelling results with advanced cubic equations of state, Fluid Phase Equilib. 428 (2016) 18–31.

[25] F.H. Verhoek, F. Daniels, The dissociation constants of nitrogen tetroxide and of nitrogen trioxide, J. Am. Chem. Soc. 53 (1931) 1250–1263.

[26] M. Cher, Rate of dissociation of N_2O_4 by ultrasonic absorption measurements, J. Chem. Phys. 37 (1962) 2564–2570.

[27] L. Harris, K.L. Churney, Evaluation of the equilibrium constant for the N_2O_4(g)=2NO_2(g) reaction at 298.16 K from light-transmission measurements, J. Chem. Phys. 47 (1967) 1703–1709.

[28] A.Z. Panagiotopoulos, Gibbs ensemble techniques, in: M. Baus, L.F. Rull, J.-P. Ryckaert (Eds.), Observation, Prediction and Simulation of Phase Transitions in Complex Fluids, Springer, Netherlands, 1995, pp. 463–501.

[29] W.R. Smith, B. Triska, The reaction ensemble method for the computer simulation of chemical and phase equilibria. I. Theory and basic examples, J. Chem. Phys. 100 (1994) 3019–3027.

[30] J.J. Potoff, A.Z. Panagiotopoulos, Critical point and phase behavior of the pure fluid and a Lennard-Jones mixture, J. Chem. Phys. 109 (1998) 10914–10920.

[31] J.J. Potoff, J.R. Errington, A.Z. Panagiotopoulos, Molecular simulation of phase equilibria for mixtures of polar and non-polar components, Mol. Phys. 97 (1999) 1073–1083.

[32] A.Z. Panagiotopoulos, Monte Carlo methods for phase equilibria of fluids, J. Phys.: Condens. Matter 12 (2000) R25–R52.

[33] J.M. Stubbs, J.J. Potoff, J.I. Siepmann, Transferable potentials for phase equilibria. 6. United-Atom description for ethers, glycols, ketones, and aldehydes, J. Phys. Chem. B 108 (2004) 17596–17605.

[34] G.C. Boulougouris, L.D. Peristeras, I.G. Economou, D.N. Theodorou, Predicting fluid phase equilibrium via histogram reweighting with Gibbs Ensemble Monte Carlo simulations, J. Supercrit. Fluids 55 (2010) 503–509.

[35] R.A. Messerly, M.S. Barhaghi, J.J. Potoff, M.R. Shirts, Histogram-free reweighting with grand canonical Monte Carlo: Post-simulation optimization of non-bonded potentials for phase equilibria, J. Chem. Eng. Data 64 (2019) 3701–3717.

[36] D. Frenkel, B. Smit, Understanding Molecular Simulation: From Algorithms to Applications, third ed., Academic Press, San Diego, California, 2023.

[37] R. Hens, A. Rahbari, S. Caro-Ortiz, N. Dawass, M. Erdös, A. Poursaeidesfahani, H.S. Salehi, A.T. Celebi, M. Ramdin, O.A. Moultos, D. Dubbeldam, T.J.H. Vlugt, Brick-CFCMC: Open source software for Monte Carlo simulations of phase and reaction equilibria using the Continuous Fractional Component method, J. Chem. Inf. Model. 60 (2020) 2678–2682.

[38] J.S. Rowlinson, B. Widom, Molecular Theory of Capillarity, first ed., Clarendon Press, Oxford, Oxfordshire, 1982.

[39] L. Vega, E. de Miguel, L.F. Rull, G. Jackson, I.A. McLure, Phase equilibria and critical behavior of square-well fluids of variable width by gibbs ensemble Monte Carlo simulation, J. Chem. Phys. 96 (1992) 2296–2305.

[40] B. Smit, Phase diagrams of Lennard-Jones fluids, J. Chem. Phys. 96 (1992) 8639–8640.

[41] A.Z. Panagiotopoulos, Molecular simulation of phase coexistence: Finite-size effects and determination of critical parameters for two- and three-dimensional Lennard-Jones fluids, Int. J. Thermophys. 15 (1994) 1057–1072.

[42] M.G. Martin, J.I. Siepmann, Transferable potentials for phase equilibria. 1. United-atom description of n-alkanes, J. Phys. Chem. B 102 (1998) 2569–2577.

[43] J.S. Rowlinson, F.L. Swinton, Molecular Theory of Capillarity, third ed., Butterworth-Heinemann, London, UK, 1982.

[44] I. Wichterle, P.S. Chappelear, R. Kobayashi, Determination of critical exponents from measurements of binary vapor–liquid equilibrium in the neighborhood of the critical line, J. Comput. Phys. 7 (1971) 606–620.

[45] A.K. Krasin, V.B. Nesterenko, Dissociating gases: A new class of coolants and working substances for large power plants, At. Energy Rev. 9 (1971) 177–194.

[46] K. Aarset, Q. Shen, H. Thomassen, A.D. Richardson, K. Hedberg, Molecular structure of the aluminum halides, Al_2Cl_6, $AlCl_3$, Al_2Br_6, $AlBr_3$, and AlI_3, obtained by gas-phase electron-diffraction and *ab initio* molecular orbital calculations, J. Phys. Chem. A 103 (1999) 1644–1652.

[47] R.G. Barnes, S.L. Segel, Dimerization of solid group IIIB trihalides. i. bromine nuclear quadrupole resonance spectrum of $AlBr_3$, J. Chem. Phys. 25 (1956) 180.

[48] D.I.S. da Silva, M.R. Mafra, F.R. da Silva, P.M. Ndiaye, L.P. Ramos, L.C. Filho, M.L. Corazza, Liquid–liquid and vapor–liquid equilibrium data for biodiesel reaction–separation systems, Fuel 108 (2013) 269–276.

[49] D. Barbosa, M.F. Doherty, The influence of equilibrium chemical reactions on vapor—liquid phase diagrams, Chem. Eng. Sci. 43 (1988) 529–540.

[50] V. Koulocheris, M. Panteli, E. Petropoulou, V. Louli, E. Voutsas, Modeling of simultaneous chemical and phase equilibria in systems involving non-reactive and reactive azeotropes, Ind. Eng. Chem. Res. 59 (2020) 8836–8847.

[51] H.M. Polat, O.A. Moultos, T.J.H. Vlugt, Monte Carlo simulation code to perform simulations in the combined Reaction and Gibbs Ensemble, 4tu.ResearchData, 2023, http://dx.doi.org/10.4121/a3ecbf66-624a-4dde-ae50-de951bc2a069.v1.

[52] A.Z. Panagiotopoulos, M.R. Stapleton, The gibbs method for molecular-based computer simulations of phase equilibria, Fluid Phase Equilib. 53 (1989) 133–141.

[53] A.Z. Panagiotopoulos, Molecular simulation of phase equilibria: simple, ionic and polymeric fluids, Fluid Phase Equilib. 76 (1992) 97–112.

[54] A.Z. Panagiotopoulos, Direct determination of fluid phase equilibria by simulation in the Gibbs Ensemble: A review, Mol. Simul. 9 (1992) 1–23.

[55] W. Smith, R. Missen, Chemical Reaction Equilibrium Analysis: Theory and Algorithms, first ed., Wiley, New York, 1982.

[56] H.M. Polat, F. de Meyer, C. Houriez, O.A. Moultos, T.J.H. Vlugt, Solving chemical absorption equilibria using free energy and quantum chemistry calculations: Methodology, limitations, and new open-source software, J. Chem. Theory Comput. 19 (2023) 2616–2629.

[57] L.F. Rull, G. Jackson, B. Smit, The condition of microscopic reversibility in gibbs ensemble Monte Carlo simulations of phase equilibria, Mol. Phys. 85 (1995) 435–447.

[58] C.H. Turner, J.K. Brennan, M. Lísal, W.R. Smith, J.K. Johnson, K.E. Gubbins, Simulation of chemical reaction equilibria by the Reaction Ensemble Monte Carlo method: A review, Mol. Simul. 34 (2008) 119–146.

[59] T.L. Hill, An Introduction to Statistical Thermodynamics, first ed., Dower Publications Inc., New York, NY, 1986.

[60] D.A.D.A. McQuarrie, J.D. Simon, Physical Chemistry : A Molecular Approach, first ed., University Science Books, Sausalito, California, 1997.

[61] H.M. Polat, M. Zeeshan, A. Uzun, S. Keskin, Unlocking CO_2 separation performance of ionic liquid/CuBTC composites: Combining experiments with molecular simulations, Chem. Eng. J. 373 (2019) 1179–1189.

[62] R.A. Messerly, T.A. Knotts, W.V. Wilding, Uncertainty quantification and propagation of errors of the Lennard-Jones 12-6 parameters for *n*-alkanes, J. Chem. Phys. 146 (2017) 194110.

[63] W. Shi, E.J. Maginn, Continuous fractional component Monte Carlo: An adaptive biasing method for open system atomistic simulations, J. Chem. Theory Comput. 3 (2007) 1451–1463.

[64] T.W. Rosch, E.J. Maginn, Reaction ensemble Monte Carlo simulation of complex molecular systems, J. Chem. Theory Comput. 7 (2011) 269–279.

[65] H.M. Polat, H.S. Salehi, R. Hens, D.O. Wasik, A. Rahbari, F.D. Meyer, C. Houriez, C. Coquelet, S. Calero, D. Dubbeldam, O.A. Moultos, T.J.H. Vlugt, New features of the open source Monte Carlo software Brick-CFCMC: Thermodynamic integration and hybrid trial moves, J. Chem. Inf. Model. 61 (2021) 3752–3757.

[66] A. Rahbari, R. Hens, M. Ramdin, O.A. Moultos, D. Dubbeldam, T.J.H. Vlugt, Recent advances in the Continuous Fractional Component Monte Carlo methodology, Mol. Simul. 47 (2021) 804–823.

[67] H.H. Reamer, B.H. Sage, Volumetric behavior of nitrogen dioxide in the liquid phase, Ind. Eng. Chem. 44 (1952) 185–187.

[68] A. Mittasch, E. Kuss, H. Schlueter, Dichten und dampfdrucke von wäßrigen ammoniaklösungen und von flüssigem stickstofftetroxyd für das temperatur-gebiet 0° bis 60°, Z. Anorg. Allg. Chem. 159 (1927) 1–36.

[69] D.N. Seshadri, D.S. Viswanath, N.R. Kuloor, Thermodynamic properties of the system $N_2O_4 \leftrightharpoons 2\ NO_2 \leftrightharpoons 2NO + O_2$, AIChE J. 16 (1970) 420–425.